PROCEEDINGS A

royalsocietypublishing.org/journal/rspa

Research

Cite this article: Selvitella AM, Foster KL. 2025 Sharp conditions for the existence and multiplicity of smooth periodic solutions to a hybrid dynamical system for human running. *Proc. R. Soc. A* **481**: 20250096. https://doi.org/10.1098/rspa.2025.0096

Received: 31 January 2025
Accepted: 19 September 2025

Subject Areas:
applied mathematics, mathematical modelling, biomechanics

Keywords:
piecewise holonomic ordinary differential equations, terrestrial locomotion, periodic gaits, shooting method, Poincaré map, numerical simulations, human data analysis

Author for correspondence:
Alessandro Maria Selvitella
e-mail: aselvite@pfw.edu

Sharp conditions for the existence and multiplicity of smooth periodic solutions to a hybrid dynamical system for human running

Alessandro Maria Selvitella[1,2] and Kathleen Lois Foster[3]

[1]Department of Mathematical Sciences, Purdue University Fort Wayne, 2101 E Coliseum Blvd, Fort Wayne, IN 46805
[2]eScience Institute, University of Washington, 3910 15th Ave NE, Seattle, WA 98195
[3]Department of Biology, Ball State University, 2000 W University Ave, Muncie, IN 47306

AMS, 0000-0002-1620-998X

In this paper, we provide necessary and sufficient conditions for the existence and multiplicity of periodic smooth solutions to a hybrid system of differential equations that describes animal running at constant angular velocity during stance. We show that solutions to this system exist if and only if the angular velocity during stance is lower than the angular velocity of the corresponding linear harmonic oscillator and satisfies a non-resonance condition. The proof of our main theorem relies on a combination of tools from oscillation theory for ODEs, intersection theory for real plane conics and the analysis of Poincaré maps. Furthermore, we demonstrate the validity of our result with numerical simulations for combinations of parameters corresponding to periodic, resonant, and unbounded solutions. Finally, we show that our model fits accurately publicly available data on human running on different conditions, including comfortable and fast running on a treadmill and overground.

Electronic supplementary material is available online at https://doi.org/10.6084/m9.figshare.c.8061265.

THE ROYAL SOCIETY PUBLISHING

1. Introduction and main theorem

The problem of accurately modelling animal locomotion has attracted a lot of attention in the past few decades [1,2]. Many studies in robotics [2–7], biomechanics [8–12], medicine [13–15], biology [16–19] and applied mathematics [20–24] have been dedicated to uncovering the underpinnings of human locomotion through a mathematical lens. Locomotion is a complex biological phenomenon that links form, function and the environment [17,25–27], it is fundamental for survival [28–30], and it is one of the determinants of evolution, through natural selection [17,30–36]. Animals navigate their environments in a remarkably broad array of locomotor strategies and are capable of a wide range of behaviours, such as walking and running across various types of surfaces [1,17,37–40]. Movement is performed through a harmonic interaction between the nervous and the musculoskeletal system of the animal, but this is hard to describe precisely with a mathematical or physical governing law [1,2,10,24,41–43]. Many people have worked in this area, starting from the pioneering work of [44–47], who established foundational mechanics of terrestrial locomotion.

A mathematical model that aims to describe animal movement in full and rigorous detail needs to be high-dimensional, such as a large system of nonlinear differential equations, and include components describing the coupled action of the neural and musculoskeletal systems [2,42]. However, such a high-dimensional system lacks interpretability and so researchers have often relied on simpler models, called *reductionist models*, which are low-dimensional and typically describe the essential dynamics of the centre of mass (CoM) in gaits such as running [11] or walking [48]. Such low-dimensional representations of locomotion dynamics (e.g. SLIP [8]) are often used as *templates* on which to *anchor* [10] higher-dimensional representations (e.g. SLIP with knee [49]).

Among the most popular reductionist models are the inverted pendulum for walking [3,4] and the SLIP for running (flight phase) and walking (double-support) [11,48]. Although models of three-dimensional (3-D) locomotion are available [50], often researchers concentrate on two-dimensional (2-D) dynamics, as it provides a simple and still accurate description of important aspects of walking and running [11,24].

In this paper, we concentrate on the sagittal (vertical and fore-aft coordinates) dynamics of the SLIP model. The SLIP model is nonlinear, not integrable [51], and also *hybrid* in the sense that it combines discrete and continuous dynamics [2,52,53]: the SLIP model is described through different vector fields for the stance (touchdown to takeoff) and flight (takeoff to touchdown) dynamics. For hybrid systems, it is hard to determine smoothness of solutions at the junction points (touchdown and takeoff) and to prove the existence of periodic trajectories. Hybrid systems are mathematically interesting because they might have the property of self-stability [54,55], that is, they might possess periodic solutions which are asymptotically stable [20], even in the absence of actuators or dissipative forces or even if the energy of the system is conserved. Hybrid systems are not Hamiltonian and only piecewise holonomic [2,20]. The proof of existence or non-existence of periodic solutions for dynamical systems such as those derived from the pendulum equation [56–58] are classical problems that have fascinated researchers for many years. However, methods based on smoothness, such as the implicit function theorem or inverse theorem are not suitable for hybrid systems in their classical formulation, and so the proof of recurrent orbits often relies on a careful analysis of the Poincaré map.

To deal with the lack of explicit solutions of the SLIP model, researchers have looked for numerical schemes [59], which often obscure biological insights because they do not lead to explicit formulas for quantities of interest (e.g. angle swept during stance). Some approximations, such as those based on the no-gravity assumption during stance [54], have turned out to be useful in qualitatively explaining the dynamics of SLIP models, whereas other authors have developed perturbative approaches to reintroduce parameters of biological significance (with gravity) [59]. Another approach aims to construct approximations of the SLIP dynamics under certain regimes or specific environmental conditions [11,21,22,24,60,61]. Primarily, researchers have worked in the limits of small angle swept during stance and small leg compression [11]. Under the first of these

regimes, the potential energy is approximated as that of a particle fixed to move in the radial axis. Such an approximation neglects the oscillatory/angular contribution to the potential energy of the point mass in the radial dynamics while running during the stance phase.

Although the assumptions of small leg compression and of small angle swept during stance can be considered perturbative regimes and so a restriction in a mathematical sense, they are not really so biologically. In fact, many studies have shown that such hypotheses are satisfied in both animal and human running. In [62], the authors show, using different methods and many subjects of height around 180 cm, that the displacement of the CoM ranges from 5 cm to 12 cm (approx. 3 to 7%), depending on running velocities (10 to 22 km h^{-1}). In [63], the authors show that, during stance, the CoM of an experienced endurance runner (5 km in 16:20) displaces between 5 cm (25 km h^{-1}) and 8 cm (10 km h^{-1}). Other studies showed that the CoM of a runner oscillates within a range of approximately 6 cm to 10 cm (approx. 5 to 10% of leg length) [62,64–67]. In [68], authors found that the angle swept by the CoM relative to the foot during stance is small (19.2 deg) during running. In [69], the author reports small variations in the angle also for several joints (e.g. hip, knee).

In this paper, we concentrate on the approximation of the SLIP model under the regime of small angle swept during stance. We do not require small leg compression and we allow the potential energy to vary sinusoidally in time during stance. Consider the following Lagrangian hybrid system:

$$\left.\begin{aligned} & L_S(r,\dot r;t)=\frac{m}{2}(\dot r^2+r^2\omega^2)-\frac{k}{2}(l_0-r)^2-mgr\cos(\omega t), \quad r(t)<l_0 \\ \text{and} \quad & L_F(r,\dot r;t)=\frac{m}{2}\dot r^2-mgr, \quad r(t)\geq l_0, \end{aligned}\right\} \tag{1.1}$$

with $L_S:(r,\dot r;t)\in[0,l_0)\times\mathbb{R}\times\mathbb{R}\mapsto\mathbb{R}$ is the Lagrangian of the stance phase, while $L_F:(r,\dot r)\in[l_0,\mathbb{R}]\times\mathbb{R}\mapsto\mathbb{R}$ represents the Lagrangian during the flight phase. Here, l_0 represents the leg length, g is the gravity constant, m the mass of the individual, $\omega>0$ (we consider only forward motion) is the frequency, $k>0$ is the spring constant, while r and $\dot r$ are the position and velocity of the particle, respectively. This problem is interesting as it emerges as an approximation of the full SLIP model [11,21,22,24]. Indeed, the SLIP Lagrangian [1] for the stance phase is given by

$$L(r,\dot r,\phi,\dot\phi)=\frac{m}{2}(\dot r^2+r^2\dot\phi^2)-\frac{k}{2}(l_0-r)^2-mgr\sin(\phi).$$

Under the limit of constant angular velocity ($\dot\phi=\omega$), one gets $\phi(t)=\phi_0+\omega t$, which, under the assumption of small angle swept during stance, concentrates around $\phi_0=\pi/2$ (the inverted pendulum unstable equilibrium), and so $\phi(t)\simeq\pi/2+\omega t$. In this regime, we obtain

$$L=\frac{m}{2}(\dot r^2+r^2\omega^2)-\frac{k}{2}(l_0-r)^2-mgr\sin\left(\frac{\pi}{2}+\omega t\right),$$

which becomes

$$L=\frac{m}{2}(\dot r^2+r^2\omega^2)-\frac{k}{2}(l_0-r)^2-mgr\cos(\omega t),$$

and so $L\sim L_S$ during stance. The dynamics during flight is parabolic and is not approximated. The Lagrangian L reduces to a one-dimensional Lagrangian L_S because the angular equation decouples: $\dot\phi=\omega$ (0th order approximation of the angular dynamics of L). Note that, in [24], the authors proved that the regime of constant angular velocity during stance is valid and approximates accurately the sagittal plane dynamics by testing the model on a benchmark dataset [70,71] of humans of different age and physical structure running on a treadmill at different speeds. Furthermore, [24] provided conditions for the asymptotic stability of periodic trajectories for varying Froude number and showed that there are periodic trajectories of the SLIP model that are stable only in a restricted range of Froude numbers, while they become unstable for smaller or larger Froude numbers. In this manuscript, we prove the following theorem.

Theorem 1.1. *Let $k, m, l_0, g > 0$ and suppose $\omega > 0$ (forward motion). Suppose that $r(t_{TO}) = r(t_{TD}) = l_0$ and that $\dot{r}(t_{TD}) = \dot{r}_0 < 0$ with t_{TO} and t_{TD} representing the instants of touchdown and takeoff, respectively. Here $r(t)$ solves system (1.1). Then:*

(a) There exist a one-parameter family of 1-periodic solutions $r(t)$ to the Euler–Lagrange equations associated with system (1.1) such that $r \in \mathcal{C}^0(\mathbb{R})$.

(b) Suppose that $\dot{r}(t_{TO}) = -\dot{r}(t_{TD})$. Then, there exists a unique 1-periodic solution $r(t)$ to the Euler–Lagrange equations associated with system (1.1) such that $r \in \mathcal{C}^1(\mathbb{R})$ if and only if $\omega^2 < k/m$ and $k \neq 2\,m\omega^2$. The period p of this solution is given by

$$p = \frac{1}{\omega}[\tau^* + 2F\dot{\rho}(\tau^*)]$$

with

$$\tau^* = \frac{1}{\sqrt{\tilde{k} - 1}}\theta(F, \dot{\rho}_0),$$

giving the time spent during stance in each stride. Here $F = \omega^2 l_0/g$, $\dot{\rho}(\tau) = \dot{r}(\omega t)/l_0$ for every $t \in \mathbb{R}$, $\dot{\rho}_0 = \dot{\rho}(0)$, and $\theta(F, \dot{\rho}_0)$ is an explicit solution satisfying the condition

$$\frac{1}{F}\sin^2(\theta(F, \dot{\rho}_0)) + 2[1 - \cos(\theta(F, \dot{\rho}_0))] + 2\dot{\rho}_0 \sin(\theta(F, \dot{\rho}_0)) = 0.$$

This solution is stable, but not asymptotically stable, with respect to perturbations satisfying the boundary conditions.

(c) There is no 1-periodic solution $r(t)$ to the Euler–Lagrange equations associated with system (1.1) such that $r \in \mathcal{C}^2(\mathbb{R})$.

The solutions that we are considering in theorem 1.1 are 1-periodic in the sense that they repeat identically in each stride. The proof of this theorem goes as follows. Given that both the stance and the flight phases are determined by smooth vector fields with smooth solutions, existence and uniqueness of solutions is granted in each single phase independently. Therefore, we need to show smoothness only at the *junction points* (e.g. the times at which the vector fields and the Lagrangians switch). The continuity of the solutions is a direct consequence of the ballistic dynamics of the flight phase. To prove smoothness, we develop a strategy that resembles the shooting method (see figure 1), but shooting from the touchdown to the takeoff times. The proof of smoothness at the *junction points* is carried out differently for the four cases: $\omega^2 = k/m$, $\omega^2 > k/m$, $k = 2\,m\omega^2$ (resonant case) and $\omega^2 < k/m$ but $k \neq 2\,m\omega^2$. The first three cases lead to non-existence of smooth solutions and the proof is based on some functional properties of the Poincaré map, whereas the fourth case gives existence of smooth solutions. The proof of existence of smooth solutions relies on some elementary but surprising ideas from algebraic geometry and intersection theory of quadrics in the plane (e.g. Bezout's theorem). These solutions are stable in a special class of functions but not asymptotically and the proof of stability relies directly on the properties of the Poincaré map. We report numerical experiments that illustrate the validity of theorem 1.1 in the three qualitatively different cases: $\omega^2 > k/m, k \neq 2\,m\omega^2, k = 2\,m\omega^2$ and $\omega^2 < k/m$. Finally, we demonstrate that the model accurately fits human running data in multiple conditions (overground vs. treadmill and comfortable vs. fast running).

The remaining part of the paper is organized as follows. In §2, we derive the non-dimensionalized equations. The core of the proof of theorem 1.1 is in §3. Section 4 is dedicated to the numerical simulations, while §5 is dedicated to the analysis of human running data. Section 6 includes a discussion and some comments, while conclusions are given in §7.

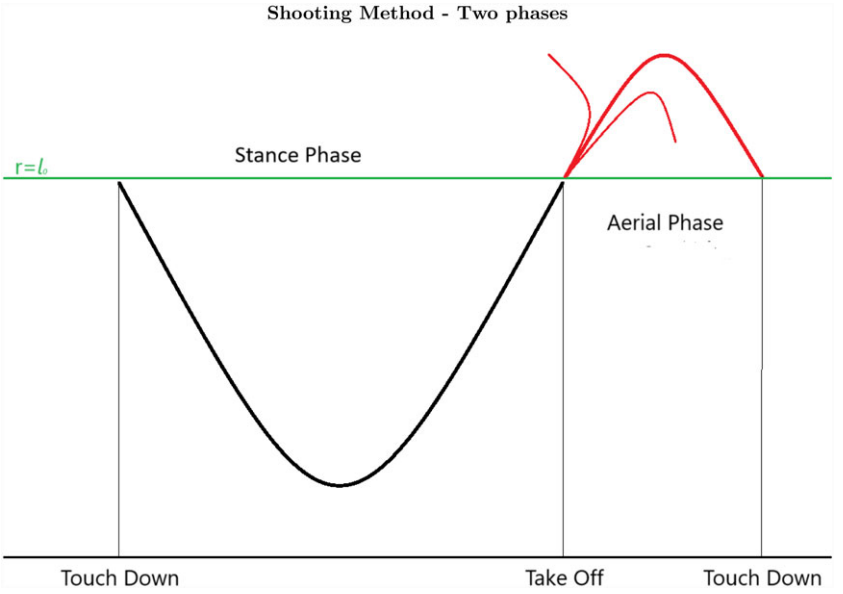

Figure 1. This figure illustrates the method used to prove existence of the solution to the hybrid system. The stance phase (black line) starts when the mass first decreases to the height $r = l_0$ (touchdown), while the aerial phase (red line) starts when the height $r = 0$ (green line) is reached again by the mass (takeoff). The additional, thinner red lines depict solutions that do not proceed periodically and do not satisfy the hypothesis of existence of $C^1(\mathbb{R})$ solutions from theorem 1.1.

2. The non-dimensionalized dynamics

In this section, we rewrite system (1.1) in normalized variables. We use this formulation for the core part of the proof in §3.

(a) Stance phase

The Euler–Lagrange equation during the stance phase $\mathrm{d}/\mathrm{d}t(\partial L_S/\partial \dot{r}) = \partial L_S/\partial r$, is given by

$$\ddot{r} = r\left[\omega^2 - \frac{k}{m}\right] + \frac{k}{m}l_0 - g\cos(\omega t).$$

Consider the following scaling:

$$\rho(t) := \frac{r(t) - l_0}{l_0}, \quad \tilde{k} := \frac{k}{m\omega^2} \quad \text{and} \quad F := \frac{\omega^2 l_0}{g},$$

which implies also $\dot{\rho} = \dot{r}/l_0$ and $\ddot{\rho} = \ddot{r}/l_0$. Note that F plays the role of the Froude number [16,17]. From this, we get

$$l_0\ddot{\rho} = [\rho l_0 + l_0]\left[\omega^2 - \frac{k}{m}\right] + \frac{k}{m}l_0 - g\cos(\omega t).$$

Simplifying, we obtain

$$\ddot{\rho} = \left(\omega^2 - \frac{k}{m}\right)\rho + \omega^2 - \frac{g}{l_0}\cos(\omega t),$$

and so

$$\frac{1}{\omega^2}\ddot{\rho} = (1 - \tilde{k})\rho + 1 - \frac{1}{F}\cos(\omega t).$$

By also scaling time,

$$t \mapsto \tau := \frac{t}{T},$$

royalsocietypublishing.org/journal/rspa Proc. R. Soc. A 481: 20250096

we obtain

$$\frac{1}{T^2\omega^2}\ddot{\rho} = (1-\tilde{k})\rho + 1 - \frac{1}{F}\cos(\omega t),$$

and so for time scales of the order $T^2 = 1/\omega^2$, (e.g. $(\omega t = \pm\tau)$) we obtain

$$\ddot{\rho} = (1-\tilde{k})\rho + 1 - \frac{1}{F}\cos(\tau),$$

and for forward motion $\omega > 0$, we get

$$\ddot{\rho} = (1-\tilde{k})\rho + 1 - \frac{1}{F}\cos(\tau). \tag{2.1}$$

Remark 2.1. With some abuse of notation, in the equations of the reduced dynamics, the derivatives are with respect to τ.

(b) Flight phase

During flight $\ddot{r} = -g$ and so $\ddot{\rho}_F = -g/l_0$. Going to the τ variable, we get $\ddot{\rho}_F = -g\omega^2/l_0$ and so the flight phase is described by

$$\ddot{\rho}(\tau) = -\frac{1}{F}.$$

Define the first *takeoff time* as

$$\tau^* = \tau^1_{TO} := \inf\{\tau > 0 \mid \rho_S(\tau) = 0\}.$$

Integrating this equation, we get

$$\rho_F(\tau) = -\frac{\tau^2}{2F} + a\tau + b,$$

with the conditions

$$\rho_F(\tau^*) = 0,$$

and the *junction condition*:

$$\dot{\rho}_F(\tau^*) = \dot{\rho}_S(\tau^*).$$

Therefore

$$\rho_F(\tau) = -\frac{\tau^2}{2F} + \left(\frac{\tau^*}{F} + \dot{\rho}_S(\tau^*)\right)\tau - \frac{\tau^{*2}}{2F} - \tau^*\dot{\rho}_S(\tau^*).$$

Hence, the two solutions are

$$\tau = \tau^* \quad \tau = \tau^* + 2F\dot{\rho}_S(\tau^*).$$

(c) Notations and preliminaries

Each stride has a potentially different τ^* and the definition of the time spent in touch with the ground can be adjusted to take this in consideration. In the proof, we denote with τ_i the touchdown time of stride i and with τ_i^* the length of the stance phase of stride i. Once τ^* is determined for the first stride (τ^1_{TO}), we need to make sure that a periodic solution with the length of each stance phase equal to τ^* ($\tau_i^* = \tau^*$ for every i) exists. We shall see that this implies that we can find a solution where each stride has the same length ($\tau_{i+1} - \tau_i$ is independent of i) and, ultimately, a 1-periodic solution. We shall also define with $v_i := \dot{\rho}_{0,i}$ the initial velocity of stride i for every i.

3. Proof of theorem 1.1

The proof of theorem 1.1 is divided in four different cases.

(a) Case $\tilde{k} = 1$

For $\tilde{k} = 1$, the equation for the stance phase becomes

$$\ddot{\rho}(\tau) = 1 - \frac{1}{F}\cos(\tau).$$

Integrating once, we obtain

$$\dot{\rho}(\tau) = \dot{\rho}_0 + \tau - \frac{1}{F}\sin(\tau),$$

and so, integrating a second time, we obtain

$$\rho(\tau) = \rho_0 + \dot{\rho}_0\tau + \frac{\tau^2}{2} + \frac{1}{F}\cos(\tau).$$

Imposing the condition that the time starts at touchdown $\tau^* = 0$ (e.g. beginning of the first stride), we have

$$\rho(0) = 0 \implies \rho_0 = -\frac{1}{F} \quad \text{and} \quad \dot{\rho}(0) = \dot{\rho}_0.$$

Therefore

$$\rho_S(\tau) = \dot{\rho}_0\tau + \frac{\tau^2}{2} - \frac{1}{F}[1 - \cos(\tau)].$$

We now look for solutions such that the takeoff time $\tau^* = 0$ corresponds to a height equal to the touchdown height $\rho(\tau^*) = 0$. Biologically, this condition corresponds to the requirement that the leg takes off when it is fully extended (note that maximum functional leg length at takeoff is distinct from the limb's anatomical maximum [72]). This is true when the following condition is satisfied:

$$\dot{\rho}_0\tau + \frac{\tau^2}{2} - \frac{1}{F}[1 - \cos(\tau)] = 0. \tag{3.1}$$

Recall that

$$\tau^* := \inf\{\tau > 0 \mid \rho_S(\tau) = 0\}.$$

For $\tilde{k} = 1$, this becomes

$$\tau^* := \inf\left\{\tau > 0 \mid \dot{\rho}_0\tau + \frac{\tau^2}{2} - \frac{1}{F}[1 - \cos(\tau)] = 0\right\}.$$

Note that τ^* in the original variables plays the role of angle swept during stance.

Lemma 3.1. *Suppose $\tilde{k} = 1$, $F > 0$, $\dot{\rho}_0 < 0$. Then there exists $\tau = \tau^* > 0$ such that $\rho(\tau^*) = 0$.*

Proof. Consider

$$y_1 := F\left[\frac{\tau^2}{2} + \dot{\rho}_0\tau\right]$$

and

$$y_2 := [1 - \cos(\tau)].$$

The lemma is proved if there exists τ such that

$$y_1(\tau) = y_2(\tau).$$

Note that

$$y_1 = 0 \leftrightarrow \tau = 0 \quad \text{or} \quad \tau = -2\dot{\rho}_0 > 0.$$

Given that $y_2 \geq 0$ and $||y_1||_{L^\infty[0,\bar{\tau}]} \nearrow \infty$ for $\bar{\tau} \nearrow +\infty$, this concludes the proof of the lemma. ∎

Remark 3.2. Note that the smaller the value of F is, the higher the number of solutions to equation (3.1). This justifies the need of using inf in the definition of τ^*. Note also that $\tau^* > -2\dot{\rho}_0$.

To verify the possibility of smooth junctions between the stance and flight phases, we check if fixed points of the Poincaré map exists in the case $\tilde{k}=1$. Note that

$$\dot{\rho}_S(\tau)=\dot{\rho}_0+\tau-\frac{1}{F}\sin(\tau),$$

which, using the condition for τ^*, becomes

$$\dot{\rho}_S(\tau)=-\frac{1}{\tau^*}\left\{\frac{\tau^{*2}}{2}-\frac{1}{F}[1-\cos(\tau^*)]\right\}+\tau-\frac{1}{F}\sin(\tau).$$

This implies that

$$\dot{\rho}_S(\tau^*)=-\frac{1}{\tau^*}\left\{\frac{\tau^{*2}}{2}-\frac{1}{F}[1-\cos(\tau^*)]\right\}+\tau^*-\frac{1}{F}\sin(\tau^*),$$

and so

$$\dot{\rho}_S(\tau^*)=\frac{\tau^*}{2}+\frac{1}{F}\left[\frac{1-\cos(\tau^*)}{\tau^*}-\sin(\tau^*)\right].$$

This implies that

$$\begin{aligned}\tau_{i+1}&=\tau_i^*+2F\dot{\rho}_S(\tau_i^*)=\tau_i^*+2F\left\{\frac{\tau_i^*}{2}+\frac{1}{F}\left[\frac{1-\cos(\tau_i^*)}{\tau_i^*}-\sin(\tau_i^*)\right]\right\}\\&=\tau_i^*(1+F)+2\left[\frac{1-\cos(\tau_i^*)}{\tau_i^*}-\sin(\tau_i^*)\right],\end{aligned}$$

with τ_i being the touchdown time of stride i and τ_i^* the length of the stance phase of stride i. Given that $v_i=\dot{\rho}_{0,i}$ and so $v_{i+1}=\dot{\rho}_F(\tau_{i+1})$, we get

$$v_{i+1}=-\frac{\tau_{i+1}}{F}+\left(\frac{\tau_i^*}{F}+\dot{\rho}_S(\tau_i^*)\right)=-\frac{\tau_i^*+2F\dot{\rho}_S(\tau_i^*)}{F}+\left(\frac{\tau^*}{F}+\dot{\rho}_S(\tau_i^*)\right)=-\dot{\rho}_S(\tau_i^*),$$

and so

$$\begin{aligned}v_{i+1}&=-\frac{\tau_i^*}{2}-\frac{1}{F}\left[\frac{1-\cos(\tau_i^*)}{\tau_i^*}-\sin(\tau_i^*)\right]=-\frac{\tau_i^*}{2}-\frac{1}{F}\left[\frac{1-\cos(\tau_i^*)}{\tau_i^*}\right]+\frac{1}{F}\sin(\tau_i^*)\\&=-\frac{\tau_i^*}{2}-\frac{1}{F}\left[\frac{1-\cos(\tau_i^*)}{\tau_i^*}\right]+\frac{1}{F}\sin(\tau_i^*),\end{aligned}$$

that is,

$$v_{i+1}=-\frac{\tau_i^*}{2}-\left[\dot{\rho}_0+\frac{\tau_i^*}{2}\right]+\frac{1}{F}\sin(\tau_i^*),$$

and so

$$v_{i+1}=-\tau_i^*-v_i+\frac{1}{F}\sin(\tau_i^*).$$

Note that at the stationary points $v_i=v$, $\tau_i^*=\tau^*$, we get

$$v=-\tau^*-v+\frac{1}{F}\sin(\tau^*),$$

and so

$$v=-\frac{\tau^*}{2}+\frac{1}{2F}\sin(\tau^*).$$

By condition (1.1), we also have

$$v\tau+\frac{\tau^2}{2}-\frac{1}{F}[1-\cos(\tau)]=0,$$

which implies

$$\frac{\tau^*\sin(\tau^*)}{2}=1-\cos(\tau^*),$$

whose solution for $\tau^* \in [0, \pi)$ is given only by $\tau^* = 0$. This concludes the proof of theorem 1.1 for the case $\tilde{k} = 1$.

(b) Case $\tilde{k} < 1$

In the case $\tilde{k} < 1$, the solutions to equation (2.1) can be written as

$$\rho(\tau) = c_+ \exp\left\{\tau\sqrt{1-\tilde{k}}\right\} + c_- \exp\left\{-\tau\sqrt{1-\tilde{k}}\right\} - \frac{1}{1-\tilde{k}} + \frac{\cos(\tau)}{F(2-\tilde{k})}.$$

We have initial conditions

$$\rho(0) = 0, \quad \dot{\rho}(0) = \dot{\rho}_0,$$

which imply

$$c_+ + c_- = \frac{1}{1-\tilde{k}} - \frac{1}{F(2-\tilde{k})}$$

and

$$c_+ - c_- = \frac{\dot{\rho}_0}{\sqrt{1-\tilde{k}}}.$$

Solving this system for c_+, c_-, this gives

$$c_+ = \frac{1}{2}\left[\frac{1}{1-\tilde{k}} - \frac{1}{F(2-\tilde{k})} + \frac{\dot{\rho}_0}{\sqrt{1-\tilde{k}}}\right] \quad \text{and} \quad c_- = \frac{1}{2}\left[\frac{1}{1-\tilde{k}} - \frac{1}{F(2-\tilde{k})} - \frac{\dot{\rho}_0}{\sqrt{1-\tilde{k}}}\right].$$

Therefore the general solution of equation (2.1) in the case $\tilde{k} < 1$ for the stance phase is given by

$$\begin{aligned}\rho_S(\tau) = {} & \frac{1}{2}\left[\frac{1}{1-\tilde{k}} - \frac{1}{F(2-\tilde{k})} + \frac{\dot{\rho}_0}{\sqrt{1-\tilde{k}}}\right] \exp\left\{\tau\sqrt{1-\tilde{k}}\right\} \\ & + \frac{1}{2}\left[\frac{1}{1-\tilde{k}} - \frac{1}{F(2-\tilde{k})} - \frac{\dot{\rho}_0}{\sqrt{1-\tilde{k}}}\right] \exp\left\{-\tau\sqrt{1-\tilde{k}}\right\} - \frac{1}{1-\tilde{k}} + \frac{\cos(\tau)}{F(2-\tilde{k})}.\end{aligned}$$

For a smooth transition at τ^*, we need the *junction conditions* to be satisfied:

$$\rho_S(\tau^*) = 0 \quad \text{and} \quad \dot{\rho}_S(\tau^*) = -\dot{\rho}_0.$$

These conditions become

$$c_+ \exp\left\{\tau^*\sqrt{1-\tilde{k}}\right\} + c_- \exp\left\{-\tau^*\sqrt{1-\tilde{k}}\right\} - \frac{1}{1-\tilde{k}} + \frac{\cos(\tau^*)}{F(2-\tilde{k})} = 0$$

and

$$c_+\sqrt{1-\tilde{k}} \exp\left\{\tau^*\sqrt{1-\tilde{k}}\right\} - c_-\sqrt{1-\tilde{k}} \exp\left\{-\tau^*\sqrt{1-\tilde{k}}\right\} - \frac{\sin(\tau^*)}{F(2-\tilde{k})} = -\dot{\rho}_0.$$

Solving the first equation for $-\dot{\rho}$, we get

$$-\dot{\rho}_0 = \frac{2\sqrt{1-\tilde{k}}}{\exp\left\{\tau^*\sqrt{1-\tilde{k}}\right\} - \exp\left\{-\tau^*\sqrt{1-\tilde{k}}\right\}} *$$

and

$$\left\{\frac{1}{2}\left[\frac{1}{1-\tilde{k}} - \frac{1}{F(2-\tilde{k})}\right]\left[\exp\left\{\tau^*\sqrt{1-\tilde{k}}\right\} + \exp\left\{-\tau^*\sqrt{1-\tilde{k}}\right\}\right] - \frac{1}{1-\tilde{k}} + \frac{\cos\tau^*}{F(2-\tilde{k})}\right\},$$

which simplifies to

$$-\dot{\rho}_0 = \frac{\sqrt{1-\tilde{k}}}{\sinh\tau^*\sqrt{1-\tilde{k}}}\left\{\left[\frac{1}{1-\tilde{k}} - \frac{1}{F(2-\tilde{k})}\right]\cosh\left(\tau^*\sqrt{1-\tilde{k}}\right) - \frac{1}{1-\tilde{k}} + \frac{\cos\tau^*}{F(2-\tilde{k})}\right\}.$$

For stance phase i, this becomes

$$-v_{i+1} = \frac{\sqrt{1-\tilde{k}}}{\sinh \tau_i^* \sqrt{1-\tilde{k}}} \left\{ \left[\frac{1}{1-\tilde{k}} - \frac{1}{F(2-\tilde{k})} \right] \cosh\left(\tau_i^* \sqrt{1-\tilde{k}}\right) - \frac{1}{1-\tilde{k}} + \frac{\cos \tau_i^*}{F(2-\tilde{k})} \right\}.$$

Analogously to the case $\tilde{k} = 1$, we have $v_{i+1} = -\dot{\rho}_S(\tau_i^*)$, which in this case is

$$\dot{\rho}_S(\tau^*) = \left[\frac{1}{1-\tilde{k}} - \frac{1}{F(2-\tilde{k})} \right] \sqrt{1-\tilde{k}} \sinh \tau^* \sqrt{1-\tilde{k}} + \dot{\rho}_0 \cosh \tau^* \sqrt{1-\tilde{k}} - \frac{\sin \tau^*}{F(2-\tilde{k})},$$

which for stance phase i, becomes

$$v_{i+1} = \left[\frac{1}{1-\tilde{k}} - \frac{1}{F(2-\tilde{k})} \right] \sqrt{1-\tilde{k}} \sinh \tau_i^* \sqrt{1-\tilde{k}} + v_i \cosh \tau_i^* \sqrt{1-\tilde{k}} - \frac{\sin \tau_i^*}{F(2-\tilde{k})}.$$

For periodic solutions, we need $v_i = v$ and $\tau_i^* = \tau^*$ for every i. Putting together the two equations for v_{i+1}, we obtain

$$\left[\frac{1}{1-\tilde{k}} - \frac{1}{F(2-\tilde{k})} \right] \sqrt{1-\tilde{k}} \sinh \tau_i^* \sqrt{1-\tilde{k}} + v_i \cosh \tau_i^* \sqrt{1-\tilde{k}} - \frac{\sin \tau_i^*}{F(2-\tilde{k})} =$$
$$- \frac{\sqrt{1-\tilde{k}}}{\sinh \tau_i^* \sqrt{1-\tilde{k}}} \left\{ \left[\frac{1}{1-\tilde{k}} - \frac{1}{F(2-\tilde{k})} \right] \cosh\left(\tau_i^* \sqrt{1-\tilde{k}}\right) - \frac{1}{1-\tilde{k}} + \frac{\cos \tau_i^*}{F(2-\tilde{k})} \right\}.$$

Multiplying both sides by $\sinh \tau_i^* \sqrt{1-\tilde{k}}(1 + \cosh \tau_i^* \sqrt{1-\tilde{k}})$, and simplifying, we obtain

$$\frac{1-\cos \tau^*}{\sin \tau^*} = \frac{\sinh \tau^* \sqrt{1-\tilde{k}}}{(1+\cosh \tau^* \sqrt{1-\tilde{k}})\sqrt{1-\tilde{k}}}.$$

If we define

$$y_1(\tau^*) := \frac{1-\cos \tau^*}{\sin \tau^*}$$

and

$$y_2(\tau^*) := \frac{\sinh \tau^* \sqrt{1-\tilde{k}}}{(1+\cosh \tau^* \sqrt{1-\tilde{k}})\sqrt{1-\tilde{k}}},$$

we notice that

$$\lim_{\tau^* \to 0} y_1(\tau^*) = \lim_{\tau^* \to 0} y_2(\tau^*) = 0,$$

but that

$$\dot{y}_1(\tau^*) = \frac{1}{1+\cos(\tau^*)} > \frac{1}{1+\cosh(\tau^*)} = \dot{y}_2(\tau^*),$$

for any $\tau^* \in (0, \pi)$. And so the only solution for $\tau^* \in [0, \pi)$ in the case $\tilde{k} < 1$ is given by $\tau^* = 0$. This concludes the proof of theorem 1.1 for the case $\tilde{k} < 1$.

(c) Case $\tilde{k} = 2$

This case is the case in which the forcing term is resonant. A general solution to equation (2.1) is then

$$\rho(\tau) = c_1 \cos(\tau) + c_2 \sin(\tau) + 1 - \frac{\tau \sin \tau}{F}.$$

Given the initial conditions

$$\rho(0) = 0 \quad \text{and} \quad \dot{\rho}(0) = \dot{\rho}_0,$$

we find

$$c_1 + 1 = 0 \quad \text{and} \quad c_2 = \dot{\rho}_0$$

and so

$$\rho(\tau) = -\cos(\tau) + \dot{\rho}_0 \sin(\tau) + 1 - \frac{\tau \sin \tau}{F}.$$

The *junction conditions* give

$$0 = -\cos(\tau^*) + \dot{\rho}_0 \sin(\tau^*) + 1 - \frac{\tau^* \sin \tau^*}{F}, \quad -\dot{\rho}_0 = \sin \tau^* + \dot{\rho}_0 \cos \tau^* - \frac{\sin \tau^* + \tau^* \cos \tau^*}{F}.$$

Solving for $1/F$ and noticing that we are interested only in the case $\tau^* > 0$ (and so ratios between the two sides of the equations can be taken), we get

$$[\sin \tau^* + \tau^* \cos \tau^*][-\cos(\tau^*) + \dot{\rho}_0 \sin(\tau^*) + 1] = \tau^* \sin \tau^* [\dot{\rho}_0(1 + \cos \tau^*) + \sin \tau^*].$$

Simplifying, we get the condition

$$[\sin \tau^* - \tau^*][1 - \cos \tau^* + \dot{\rho}_0 \sin \tau^*] = 0.$$

Since we have already considered the case $\tau^* = 0$, this implies

$$\dot{\rho}_0 = \frac{\cos \tau^* - 1}{\sin \tau^*}.$$

If we substitute this back in the first *junction condition*, we obtain

$$0 = -\cos(\tau^*) + \frac{\cos \tau^* - 1}{\sin \tau^*} \sin(\tau^*) + 1 - \frac{\tau^* \sin \tau^*}{F},$$

which implies $\tau^* = 0$ or $\tau^* = \pi$, and $\tau^* = 0$ satisfies the second *junction condition*, but $\tau^* = \pi$ gives $0 = 1/F$, which is a contradiction. This concludes the proof of theorem 1.1 for the case $\tilde{k} = 2$, that is, $k = 2\,\mathrm{m}\omega^2$.

(d) Case $\tilde{k} > 1$ and $\tilde{k} \neq 2$

In this case, the general solution to equation (2.1) is given by

$$\rho(\tau) = c_1 \cos(\tau\sqrt{\tilde{k} - 1}) + c_2 \sin(\tau\sqrt{\tilde{k} - 1}) + \frac{1}{\tilde{k} - 1} - \frac{\cos(\tau)}{F(\tilde{k} - 2)},$$

with the initial conditions

$$\rho(0) = 0 \quad \text{and} \quad \dot{\rho}(0) = \dot{\rho}_0.$$

These two conditions imply

$$0 = c_1 + \frac{1}{\tilde{k} - 1} - \frac{1}{F(\tilde{k} - 2)}$$

and

$$\dot{\rho}_0 = c_2\sqrt{\tilde{k} - 1}.$$

Therefore, we obtain

$$\rho(\tau) = \left[\frac{1}{F(\tilde{k} - 2)} - \frac{1}{\tilde{k} - 1}\right] \cos\left(\tau\sqrt{\tilde{k} - 1}\right) + \frac{\dot{\rho}_0}{\sqrt{\tilde{k} - 1}} \sin(\tau\sqrt{\tilde{k} - 1}) + \frac{1}{\tilde{k} - 1} - \frac{\cos(\tau)}{F(\tilde{k} - 2)}.$$

Note that also here, we are looking for τ^* such that the *junction conditions* are satisfied: $\rho(\tau^*) = 0$ and $\dot{\rho}(\tau^*) = -\dot{\rho}_0$. Define the auxiliary variables $Y := \sin(\tau^*\sqrt{\tilde{k} - 1})$ and $X := \cos(\tau^*\sqrt{\tilde{k} - 1})$. Then,

the *junction conditions* become

$$\left.\begin{aligned} c_2Y + c_1X &= \frac{\cos(\tau^*)}{F(\tilde{k}-2)} - \frac{1}{\tilde{k}-1} =: F_1(\tau^*) \\ \text{and} \qquad -c_1Y + c_2X &= -\frac{\sin\tau^*}{F(\tilde{k}-2)\sqrt{\tilde{k}-1}} - \frac{\dot{\rho}_0}{\sqrt{\tilde{k}-1}} =: F_2(\tau^*). \end{aligned}\right\}$$

Multiplying by c_2 the first equation, by c_1 the second equation, and subtracting the second from the first equations, we obtain

$$Y = \frac{1}{c_1^2 + c_2^2}(F_1(\tau^*)c_2 - F_2(\tau^*)c_1).$$

Multiplying by c_1 the first equation, by c_2 the second equation, and summing the second and first equations, we obtain

$$X = \frac{1}{c_1^2 + c_2^2}(F_1(\tau^*)c_1 + F_2(\tau^*)c_2).$$

Note that

$$c_1 = F_1(0) \quad c_2 = -F_2(0),$$

with $F_1(0), F_2(0)$ meaning $F_1(\tau^* = 0), F_2(\tau^* = 0)$, respectively. Therefore,

$$\left.\begin{aligned} Y &= \frac{1}{F_1(0)^2 + F_2(0)^2}(-F_1(\tau^*)F_2(0) - F_2(\tau^*)F_1(0)) \\ \text{and} \qquad X &= \frac{1}{F_1(0)^2 + F_2(0)^2}(F_1(\tau^*)F_1(0) - F_2(\tau^*)F_2(0)). \end{aligned}\right\}$$

Since $Y^2 + X^2 = 1$, then

$$[F_1(0)^2 + F_2(0)^2]^2 = [F_1(\tau^*)F_2(0) + F_2(\tau^*)F_1(0)]^2 + [F_1(\tau^*)F_1(0) - F_2(\tau^*)F_2(0)]^2,$$

which simplifies to

$$F_1(0)^2 + F_2(0)^2 = F_1(\tau^*)^2 + F_2(\tau^*)^2,$$

since $F_1(0)^2 + F_2(0)^2 \neq 0$ (this is true because $\dot{\rho}_0 < 0$). This condition is in fact a system of quadratic equations of the form

$$\left.\begin{aligned} \Gamma_1 &: \quad X^2 + Y^2 - 1 = 0 \\ \text{and} \qquad \Gamma_2 &: \quad \left(\frac{X}{a_1} - b_1\right)^2 + \left(\frac{Y}{a_2} - b_2\right)^2 = \left(\frac{1}{a_1} - b_1\right)^2 + b_2^2, \end{aligned}\right\} \tag{3.2}$$

with

$$a_1 = F(\tilde{k}-2), \quad a_2 = F(\tilde{k}-2)\sqrt{\tilde{k}-1}, \quad b_1 = \frac{1}{\tilde{k}-1}, \quad b_2 = -\frac{\dot{\rho}_0}{\sqrt{\tilde{k}-1}}.$$

Note that the point $(W, Z) = (1, 0)$ solves the system and corresponds to the case $\tau^* = 0$. Note that this intersection point has multiplicity greater than 1 if and only if the tangents of the two curves at $(X, Y) = (1, 0) =: P$ are the same. Therefore, we check conditions for which the tangent at P to Γ_1 intersects Γ_2 transversally. We have

$$\left(\frac{1}{a_1} - b_1\right)^2 + \left(\frac{Y}{a_2} - b_2\right)^2 = \left(\frac{1}{a_1} - b_1\right)^2 + b_2^2,$$

and so

$$\frac{Y}{a_2}\left(\frac{Y}{a_2} - 2b_2\right) = 0.$$

The first solution is then $Y = 0$ which corresponds to the case $\tau^* = 0$, while the second solution is

$$Y = 2a_2b_2 = -2\frac{\dot{\rho}_0}{\sqrt{\tilde{k}-1}}F(\tilde{k}-2)\sqrt{\tilde{k}-1} = -2\dot{\rho}_0F(\tilde{k}-2).$$

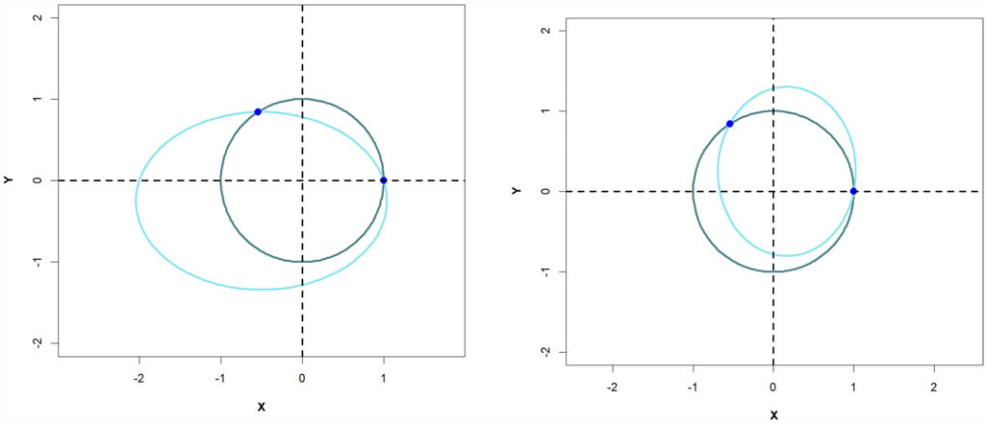

Figure 2. This figure displays the intersection $\Gamma_1 \cap \Gamma_2$ in the case $\dot{\rho}_0 = 1$, $F = 0.5$, and $\tilde{k} = 1.5$ (left) and $\tilde{k} = 2.5$ (right). This figure serves as an illustration of the last step of the proof of theorem 1.1, that is, that $0 < \tau^* < \pi$.

This expression is not zero, since we are in the case $\tilde{k} > 1$, $\tilde{k} \neq 2$ and $\dot{\rho}_0 < 0$.

Suppose $\tilde{k} < 2$, then the centre of the ellipse Γ_2 has both coordinates negative. Therefore Γ_2 passes through P in its upper-right quadrant and so it cuts Γ_1 at P with a negative tangent. This means that Γ_2 intersect Γ_1 at a second point $Q \neq P$ with $Y > 0, X \neq -1$. This implies that there exists τ^* such that $0 < \tau^* < \pi$ that satisfies the *junction conditions*. On the other side, for $\tilde{k} > 2$ the centre of the ellipse Γ_2 has both coordinates positive, but, for analogous reasons, also in this case there exists τ^* such that $0 < \tau^* < \pi$ that satisfies the *junction conditions*. In fact, also in this case, Γ_2 intersects Γ_1 at two distinct points: P which corresponds to $\tau^* = 0$ and a second point $Q \neq P$, which corresponds to $\tau^* > 0$. Note that, since $b_1 > 0$ and $b_2 > 0$, also $\tau^* < \pi$. Therefore, also in the case $\tilde{k} > 1, \tilde{k} \neq 2$, there exists $\tau^* \in (0, \pi)$ satisfying the *junction conditions* (see figure 2 for an illustration of this). This concludes the proof of theorem 1.1 for the case $\tilde{k} > 1$, $\tilde{k} \neq 2$.

(i) Length of the stance phase

For now, let us fix $\theta := \tau^* \sqrt{\tilde{k} - 1}$. By substituting $Y := \sin(\theta)$ and $X := \cos(\theta)$ into the equation for Γ_2, we obtain

$$\frac{\cos^2(\theta)}{a_1^2} + \frac{\sin^2(\theta)}{a_2^2} - 2\frac{b_1}{a_1}\cos(\theta) - 2\frac{b_2}{a_2}\sin(\theta) + 2\frac{b_1}{a_1} - \frac{1}{a_1^2} = 0.$$

Simplifying further, we find that

$$\frac{\cos^2(\theta) - 1}{a_1^2} + \frac{\sin^2(\theta)}{a_2^2} 2\frac{b_1}{a_1}[1 - \cos(\theta)] - 2\frac{b_2}{a_2}\sin(\theta) = 0,$$

and so

$$\frac{-\sin^2(\theta)}{a_1^2} + \frac{\sin^2(\theta)}{a_2^2} 2\frac{b_1}{a_1}[1 - \cos(\theta)] - 2\frac{b_2}{a_2}\sin(\theta) = 0,$$

which implies

$$\left(\frac{1}{a_2^2} - \frac{1}{a_1^2}\right)\frac{\sin^2(\theta)}{a_2^2} + 2\frac{b_1}{a_1}[1 - \cos(\theta)] - 2\frac{b_2}{a_2}\sin(\theta) = 0.$$

Note that

$$\left(\frac{1}{a_2^2}-\frac{1}{a_1^2}\right)=\left(\frac{1}{[F(\tilde{k}-2)\sqrt{\tilde{k}-1}]^2}-\frac{1}{[F(\tilde{k}-2)]]^2}\right)=\frac{1}{F^2[\tilde{k}-2]^2}\left(\frac{1}{\tilde{k}-1}-1\right)$$
$$=\frac{1}{F^2[\tilde{k}-2]^2}*\left(\frac{\tilde{k}-2}{\tilde{k}-1}\right)=\frac{1}{F^2(\tilde{k}-2)(\tilde{k}-1)}=\frac{1}{F}\frac{b_1}{a_1}.$$

On the other side

$$\frac{b_2}{a_2}=-\frac{\frac{\dot{\rho}_0}{\sqrt{\tilde{k}-1}}}{F(\tilde{k}-2)\sqrt{\tilde{k}-1}}=-\dot{\rho}_0\frac{b_1}{a_1}.$$

Therefore,

$$0=\left(\frac{1}{a_2^2}-\frac{1}{a_1^2}\right)\frac{\sin^2(\theta)}{a_2^2}+2\frac{b_1}{a_1}[1-\cos(\theta)]-2\frac{b_2}{a_2}\sin(\theta)$$
$$=\left(\frac{1}{a_2^2}-\frac{1}{a_1^2}\right)\frac{\sin^2(\theta)}{a_2^2}+2\frac{b_1}{a_1}[1-\cos(\theta)]-2\frac{b_2}{a_2}\sin(\theta)$$
$$=\frac{1}{F}\frac{b_1}{a_1}\sin^2(\theta)+2\frac{b_1}{a_1}[1-\cos(\theta)]+2\dot{\rho}_0\frac{b_1}{a_1}\sin(\theta).$$

Given that $\frac{b_1}{a_1}\neq 0$, then

$$\frac{1}{F}\sin^2(\theta)+2[1-\cos(\theta)]+2\dot{\rho}_0\sin(\theta)=0.$$

Note that for this formula to be valid, we require $\sin(\theta)>0$, as $\dot{\rho}_0<0$. This corresponds to one assumption of theorem 1.1 and to the fact that $0<\tau^*<\pi$. In this range, we can use parametric formulas for trigonometric functions. Therefore, by substituting parametric formulas for $\sin(\theta)$ and $\cos(\theta)$, so that $\sin(\theta)=2t/1+t^2$ and $\cos(\theta)=1-t^2/1+t^2$ with $t=\tan(\theta/2)$, one could reduce this equation to a polynomial of 4th order in t with one solution $t=0$. The cubic factor of such polynomial will have a second solution $\theta\neq 0$. This implies that

$$\tau^*\sqrt{\tilde{k}-1}=\theta=\theta(F,\dot{\rho}_0),$$

and so

$$\tau^*=\frac{1}{\sqrt{\tilde{k}-1}}\theta(F,\dot{\rho}_0).$$

The function $\theta(F,\dot{\rho}_0)$ can be explicitly computed, but the expression is convoluted and so we do not report it here.

Proof. Because of the regularity of the vector fields in each of the two phases, the solution in each phase is unique, given the conditions at touchdown and takeoff. Once a solution to the stance phase satisfying the conditions $r(t_{TO})=r(t_{TD})=l_0$, $\dot{r}(t_{TD})=\dot{r}_0<0$, and $\dot{r}(t_{TO})=-\dot{r}(t_{TD})$ is found, the solution to the aerial phase will automatically provide conditions for transition to the next stride, simply because of the symmetry of the parabolic motion.

Part (a). This is a consequence of the fact that ρ_F is a parabola (concave down) and it reaches its maximum at $\tau_m=\tau^*+\dot{\rho}_S(\tau^*)$, which implies $\rho_F(\tau_m)=\dot{\rho}_S(\tau^*)/2>0$. Therefore, ρ_F intersects two times $\rho=0$. Note that no condition is imposed to the velocity at the junction points and so there exists a one-parameter family of continuous solutions.

Part (b). Since for every $\tilde{k}>1$ and $\tilde{k}\neq 2$, there exists $\tau^*>0$ satisfying the *junction conditions* (see above), the solution to equation (2.1) is smooth at τ^* and so it is smooth everywhere. Going back to the original variables, this implies that for $\omega^2<k/m$ and $k\neq 2\,\mathrm{m}\omega^2$, the corresponding $r(t)$ is a $\mathcal{C}^1$ solution to system (1.1). Note that there is only one solution satisfying the first (and so all) *junction conditions* and it is 1-periodic by construction. This solution is unique because of uniqueness in each single phase and uniqueness of the solution satisfying the *junction conditions* for 1-periodic solutions.

By the derivation in §2b, the length of the flight phase in normalized coordinates is $2F\rho_S(\tau^*)$, while by the derivations in §3d(i), the length of the stance phase in normalized coordinates is

$$\tau^* = \frac{1}{\sqrt{\tilde{k}-1}}\theta,$$

with θ an explicit solution satisfying

$$\frac{1}{F}\sin^2(\theta) + 2[1-\cos(\theta)] + 2\dot{\rho}_0\sin(\theta) = 0.$$

Therefore, in normalized coordinates, the period of our solution is

$$\tau^* + 2F\rho_S(\tau^*).$$

Rewriting this is the non-scaled variables, we have the formula for the period p stated in the theorem.

Since for 1-periodic solutions the *junction conditions* are satisfied and because the flight phase is uniquely determined by the conditions at takeoff/touchdown, then we have that consecutive heights satisfy $\rho_{i+1} = \rho_i$ and so the Poincaré map is the identity map in the space of functions satisfying the boundary conditions. Therefore, these solutions are stable but not asymptotically stable in this space.

Since the *junction conditions* are not satisfied for $\tilde{k} < 1$, then the corresponding $r(t)$ is not a $\mathcal{C}^1$ solution to system (1.1) for $\omega^2 \geq k/m$.

Part (c). At takeoff, a solution to be $\mathcal{C}^2$ needs $\ddot{\rho}_F(\tau^*) = \ddot{\rho}_S(\tau^*)$, that is,

$$-\frac{1}{F} = (1-\tilde{k})\rho(\tau^*) + 1 - \frac{1}{F}\cos(\tau^*),$$

which, after simplifying, becomes

$$\frac{1}{F}\cos(\tau^*) = 1 + \frac{1}{F} > \frac{1}{F},$$

which is impossible. Therefore, no solution to system (1.1) can be $\mathcal{C}^2$.

This completes the proof of theorem 1.1. ■

4. Numerical simulations

This section is dedicated to some numerical experiments. In particular, we simulate solutions to system (1.1) in the three relevant cases: figure 3 is dedicated to the case $\omega^2 < k/m$, $k \neq 2\,\mathrm{m}\omega^2$ (periodic case, see theorem 1.1), figure 4 is dedicated to the case $k = 2\,\mathrm{m}\omega^2$ (resonant case, see theorem 1.1) and figure 5 is dedicated to the case $\omega^2 > k/m$ (exponential case, see theorem 1.1). In each plot, we depict the time series of mass displacement, mass velocity and mass acceleration, for a vector of parameters belonging to the appropriate, corresponding range. The experiments have been performed using *Python* libraries *numpy*, *matplotlib*, *scipy*, and solutions to system (1.1) have been simulated using the function *solve_ivp* from *scipy*. The function *solve_ivp* does not directly provide output of the acceleration; this was computed by taking the first difference of the velocity and rescaling it by the number of collocation points and the length of the time interval chosen for the simulation. This procedure is good, but the plot show some numerical artefact in the acceleration plots around the *junction points*, where the dynamics switches from the stance to the aerial phase.

In support of our main theoretical result, theorem 1.1, the only periodic solution is the one simulated in the case $\omega^2 < k/m$, $k \neq 2\,\mathrm{m}\omega^2$ and plotted in figure 3. The simulation of the solution in the resonant case $k = 2\,\mathrm{m}\omega^2$ shows secular terms (figure 4), while the solution plotted in figure 5 shows an unbounded solution (case $\omega^2 < k/m$).

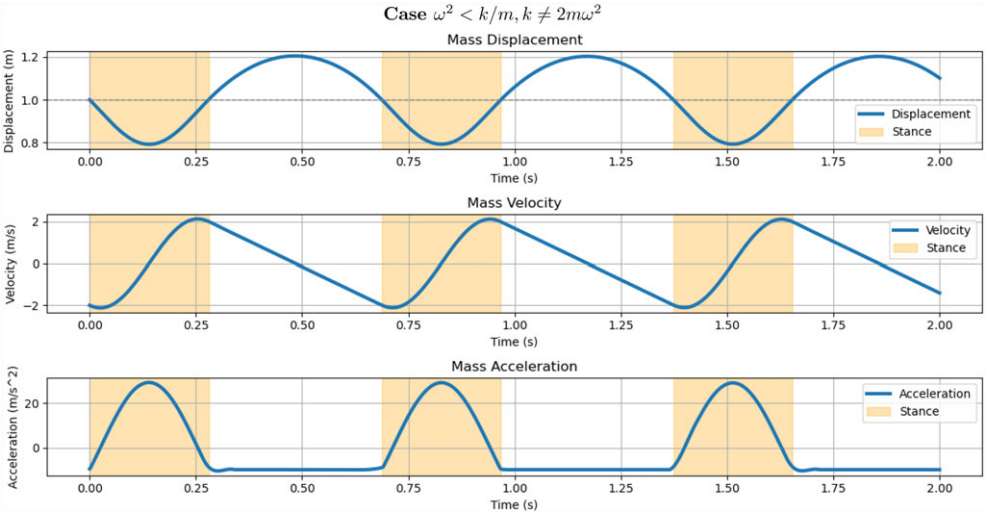

Figure 3. This figure displays mass displacement, velocity and acceleration in the case $\omega^2 < k/m$ and $k \neq 2m\omega^2$. This is the case that admits periodic solutions (see theorem 1.1). The time span is $t \in [0, 2]$, with parameters $g = 9.81\,\mathrm{m\,s^{-2}}$, $l_0 = 1\,\mathrm{m}$, $k = 15000\,\mathrm{N\,m^{-1}}$, $m = 80\,\mathrm{kg}$ and $\omega = 0.02\,\mathrm{rad\,s^{-1}}$. The stance phase is indicated by the shaded regions. The beginning of the shaded regions corresponds to the touchdown time, while the end of the shaded regions corresponds to the takeoff time.

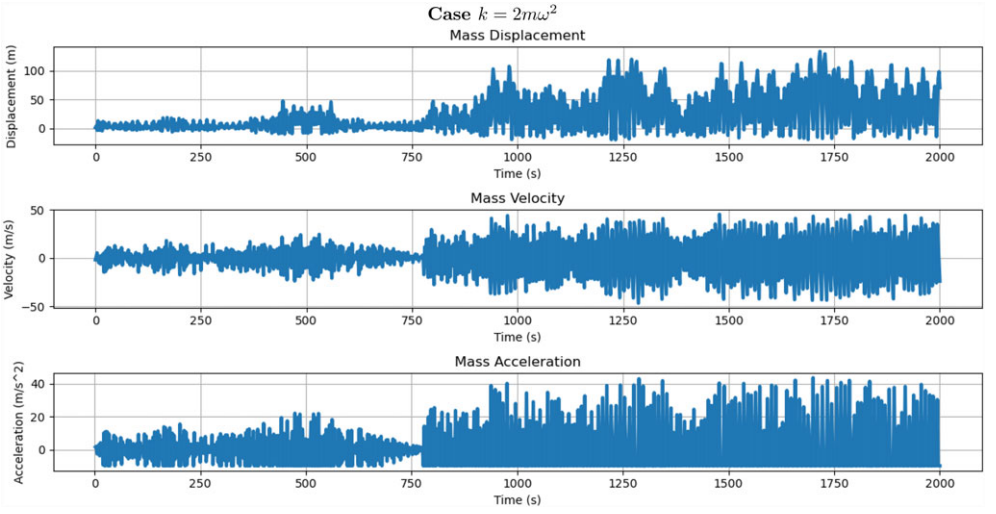

Figure 4. This figure displays mass displacement, velocity and acceleration in the case $k = 2\,m\omega^2$. This is the case that involves resonant/secular solutions (see theorem 1.1). The time span is $t \in [0, 2000]$, with parameters $g = 9.81\,\mathrm{m\,s^{-2}}$, $l_0 = 1\,m$, $k = 640\,\mathrm{N\,m^{-1}}$, $m = 80\,\mathrm{kg}$ and $\omega = 2\,\mathrm{rad\,s^{-1}}$.

5. Human running data model fitting

We test our models on publicly available data of human running, available from [73,74]. This dataset includes the 3-D landmarks time series of 30 healthy young individuals aged between 21 and 41 years and includes both walking and running experiments, divided in two sessions. For our purposes only running experiments from session 1 are used. Individuals run at comfortable and fast speeds on both overground and treadmill. The time series of the CoM dynamics is already

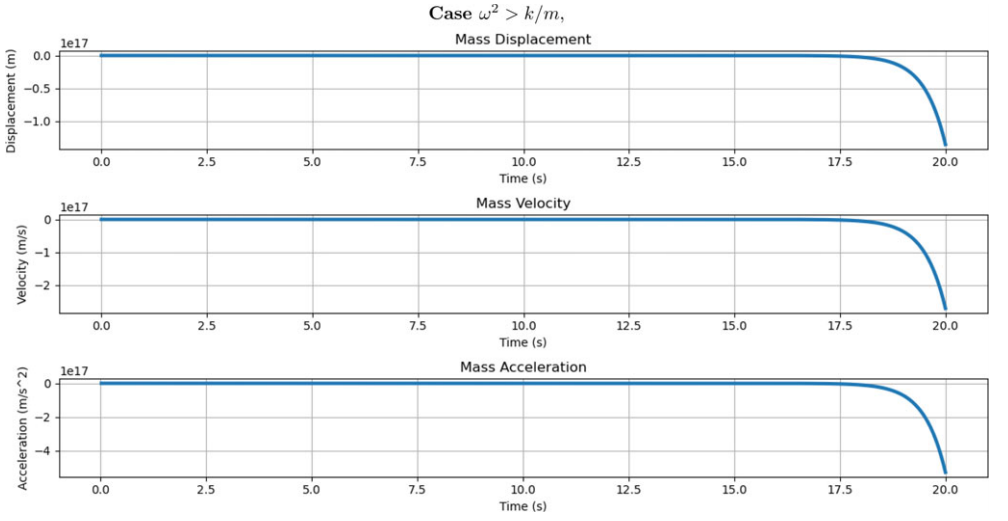

Figure 5. This figure displays mass displacement, velocity and acceleration in the case $\omega^2 > k/m$. This is the case that produces exponential solutions (see theorem 1.1). The time span is $t \in [0, 20]$, with parameters $g = 9.81\,\mathrm{m\,s^{-2}}$, $l_0 = 1\,\mathrm{m}$, $k = 1\,\mathrm{N\,m^{-1}}$, $m = 80\,\mathrm{kg}$ and $\omega = 2\,\mathrm{rad\,s^{-1}}$.

computed by the authors of [73,74]. The measurements are taken following the conventional gait model, where the coordinates are given by: X-axis in the posterior–anterior direction, the Y-axis oriented left to right with respect to the direction of locomotion, and the Z-axis in the vertical direction (opposite to gravity). We refer to [73,74] for more information about how the data was collected and processed.

The data analysis reported here considers one individual (ID LD002, male) and includes multiple strides and both stance and aerial phases in each of the conditions analysed (4: treadmill vs. overground and comfortable vs. fast pace). We measure the distance between r_{data}, the available measurements, and r_{fitted}, the fitted measurements, in terms of the relative error e_{rel} of the L^∞ norm:

$$e_{\text{rel}} := \frac{||r_{\text{data}}(t) - r_{\text{fitted}}(t)||_{L^\infty[t_{TD},t_{TO}]}}{||r_{\text{data}}(t)||_{L^\infty[t_{TD},t_{TO}]}},$$

where $||f(t)||_{L^\infty[a,b]} := \sup_{t\in[a,b]} |f(t)|$, similar to how errors were measured in [21,24].

The mass of this individual (85 kg) is provided in the metadata file from [73,74]. The data are fitted using the *curve_fit* function from the *scipy.optimize* Python package. The optimization algorithm we used is Levenberg–Marquardt and it was initialized with the values listed in table 1. The parameters provided to the algorithm are g, the gravity constant, l_0, the touchdown height and m, the mass of the individual. The fitted parameters are the stiffness k and ω. The model is second order in time, so it needs initial conditions for both the displacement and the velocity. The initial condition for the displacement was given by the first observation in the time series, while the initial velocity was given by the first difference of the first two observations normalized by the time step $t_{\text{step}} = 0.01$. The results of our analysis are shown in figure 6. The picture shows the time series of the observations and of the fitted values and reports the relative error e_{rel} in the four cases analysed. In all cases we analysed $e_{\text{rel}} < 10\%$.

We further tested our model on another subject with different features: Subject BD004 (female, $m = 53$ *kg*) from the same dataset [73,74] on overground comfortable (initial values for optimization: $k = 20\,000$ and $\omega = 0.01$) and fast running (initial values for optimization: $k = 20\,000$ and $\omega = 0.1$). Also in these cases, $e_{\text{rel}} < 10\%$. The results of this additional analysis are shown in figure 7.

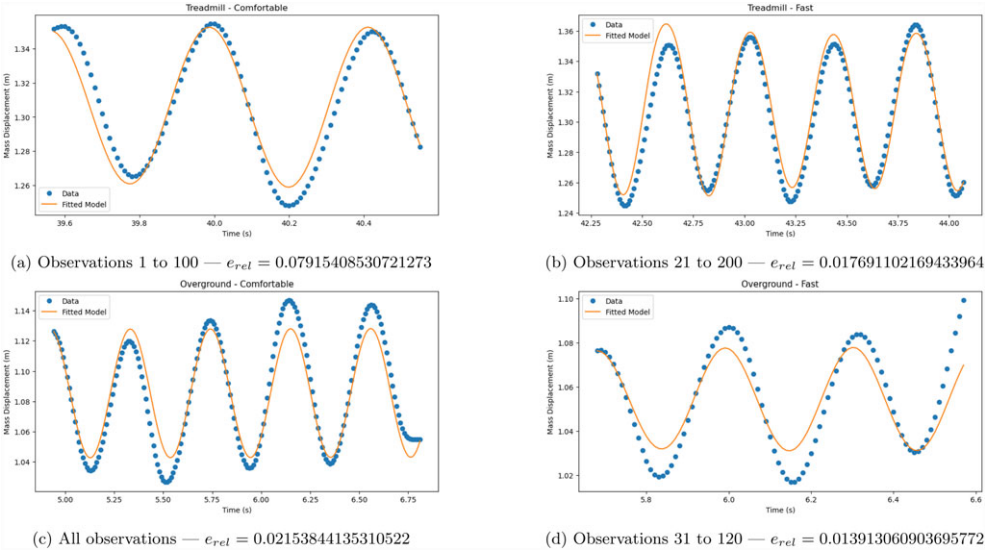

(a) Observations 1 to 100 — $e_{rel} = 0.07915408530721273$
(b) Observations 21 to 200 — $e_{rel} = 0.017691102169433964$
(c) All observations — $e_{rel} = 0.02153844135310522$
(d) Observations 31 to 120 — $e_{rel} = 0.013913060903695772$

Figure 6. This picture shows the post-processed recorded data of session 1 of the experiments of comfortable and fast running on a treadmill (left to right, top row) and of comfortable and fast running overground (left to right, bottom row) of subject LD002 (male, $m = 85$ kg) from the publicly available dataset [73,74]. The captions of each subfigure report the observations considered in the model fitting and the error measured in terms of e_{rel}.

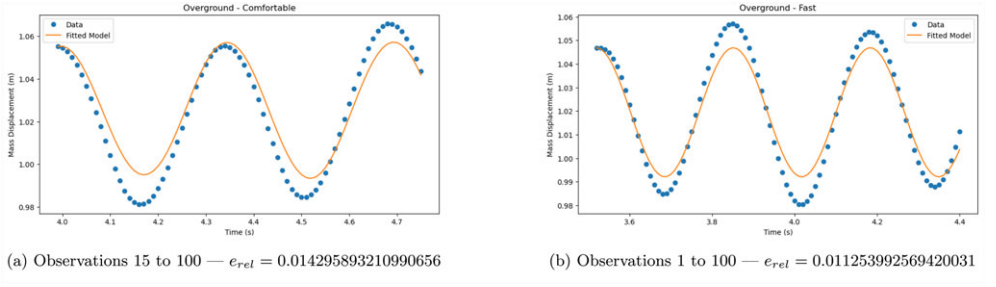

(a) Observations 15 to 100 — $e_{rel} = 0.014295893210990656$
(b) Observations 1 to 100 — $e_{rel} = 0.011253992569420031$

Figure 7. This figure shows the post-processed recorded data of session 1 of the experiments of comfortable and fast running overground (left to right, bottom row) of subject BD004 (female, $m = 53$ kg) from the publicly available dataset [73,74]. The captions of each subfigure report the observations considered in the model fitting and the error measured in terms of e_{rel}.

Table 1. Initial values for the optimization algorithm in the four conditions (T=treadmill, O=overground; C=comfortable, F=fast).

parameters	T-C	T-F	O-C	O-F
k	12 000	22 000	20 000	28 000
ω	0.01	0.02	0.1	0.16

6. Comments

(a) On the mathematical results

In [11,24], a correction in the horizontal velocity at takeoff is determined for the existence of periodic solutions because it allows the energy to be kept constant for asymmetric stance phases.

In particular, [11] commented on how such a manipulation was artificial. No such correction is needed in our proof of existence of periodic smooth solutions.

The proofs of non-existence for the cases $\omega^2 \geq k/m$ are based on the fact that such a condition and the *junction conditions* are incompatible. Theorem 1.1 can be considered some sort of unique continuation result: If the frequency $\omega^2 \geq k/m$, then for the motion to take place, the frequency needs to be $+\infty$, which implies that the stance phase needs to be instantaneous. In other words, if running happens at a too high a frequency, the impact of the foot with the ground needs to be collisional [1] and an impulse needs to switch velocity from $\dot{\rho}_0$ to $-\dot{\rho}_0$ instantaneously. In turn, the solution cannot be $\mathbb{C}^1$ at the *junction points*.

A direct application of Bezout's Theorem [75,76] can give explicit solutions for τ^* (in terms of the inverse of elementary functions) in the case $\omega^2 < k/m$ and $k \neq 2\,\mathrm{m}\omega^2$. The strategy boils down to finding the zeros of a resultant, a polynomial of fourth order, for which only one of the roots (corresponding to $\tau^* = 0$) is known. Once the remaining three roots (one of which is surely real and so there exists a point in the real plane $Q \neq P = (1, 0)$ that solve the resultant equation) are found, then one has to verify if any of these solutions are valid (they must satisfy $X^2 + Y^2 - 1 = 0$ in the notation of that subsection). This happens because the strategy based on the resultant loses information about the constraints on X and Y, which are trigonometric functions of τ^*. The computations to verify all of this are very involved and tedious, so we decided not to report that analysis, given also that an explicit formula for τ^* is not needed for the proof of theorem 1.1

Our result is different from that available in the literature in many aspects. In contrast with the authors in [11,21,22,24], we do not assume small leg compression, and our results are valid without that restriction. With respect to [11], we do not assume that the Froude number is such that $F = 1$ (i.e. the frequency of the system is the pendulum frequency), and our results are valid for every $F > 0$. We are not aware of other papers proving rigorous non-existence or regularity results for SLIP-based systems, whereas theorem 1.1 gives sharp conditions for the existence of smooth 1-periodic solutions. Unlike many papers in the SLIP literature [11], we do not directly assume symmetry of the stance phase; however, such a condition is basically replaced by the smoothness requirements imposed by the *junction conditions*. Furthermore, the findings of this paper augment our analysis in [24], since here we are able to give sharp conditions for the existence of smooth periodic gaits, show that the vertical displacement is correctly modelled by our reduced-SLIP dynamics, and provide exact trajectories of the CoM solving the reduced system that are explicit in terms of elementary functions.

Although, our model is one dimensional, it still relates closely to the full sagittal dynamics described by the SLIP. The original Lagrangian $L(r, \dot{r}, \phi, \dot{\phi})$ of the SLIP model is autonomous. In the regime that we are considering, time appears explicitly in the potential energy term $mgr\cos(\omega t)$. If we take the derivative of the energy of our model, that is not going to be identically zero over solutions of the Lagrange equations during stance. In our system, the potential energy acts like an external forcing. However, this forcing term oscillates and allows for the junction conditions to be satisfied under the conditions of theorem 1.1. This is not enough to match solutions of the full 2-D SLIP model to those of our model, as there needs to be a match in the angular dynamics too. The angle of attack is essentially a degree of freedom we can use to ensure that there is no loss of energy in each stride, also when we add back the angular dynamics. The quantity τ^* represents the angle swept during stance of the full 2-D SLIP model. This does not determine the initial condition of the equation $\dot{\phi} = \omega$, that is, the angle of attack, but only how much time/angle is spent in the stance phase. Given that τ^* is always between zero and π (as we prove in theorem 1.1), we can always choose an angle of attack α_0 such that the angle swept during stance is symmetric around $\pi/2$ and so there is no loss of energy per stride of the full 2-D model, as well.

Theorem 1.1 does not say anything about N-periodic solutions with $N > 1$ (solutions that repeat a group of N strides periodically, but with each stride potentially different) and so this problem remains open. Furthermore, the conditions under which we prove stability are quite restrictive and so this question remains largely open, as well.

(b) On the biological relevance and limitations

As can be seen from the results in §5 and figures 3, 4 and 5, the model fits the data considered relatively well, despite different types of conditions considered and the simplicity of the model. However, the outcome of the algorithm we used seems very sensitive to the initial values of k and ω fed to the algorithm. This is reminiscent of the slim Christmas-candy-cane-shaped stability picture of SLIP models (see [11,24]). Given the complex loss function parameter landscape the algorithm has to deal with, it is not easy determine the initial parameters that lead to optimal performance of the algorithm. The parameters fitted to the model are those that can be considered as latent or summarizing complex interactions, such as the stiffness k and the angular velocity ω, which, in this case, balance effects resulting from the angular motion during stance and the approximation error. In both figures 6 and 7, the error in the approximation seems to be mostly due to the step-by-step asymmetry in the gait and it concentrates on the peaks of the curve. As a consequence, the height of the peaks seems to be underestimated by our model. In both figures 6 and 7, the transitions between phases are smooth, as imposed by the *junction conditions*.

The choice of sub-selecting observations from the full gait highlights that sub-selecting does not necessarily improve the fit, which seems to remain similarly accurate through the gait. In turn, this underlines that each part of the gait resembles features of the full gait and so the good fit is probably related to intrinsic features of the movement captured by the model. The initial observation considered in the four examples allows us to compare the accuracy of the model between cases in which the velocity of the first observation considered is slightly positive (comfortable, treadmill) or negative (other three cases) and shows that a decrease in accuracy is present in the former case. In general, the model suffers when the different strides are more heterogeneous. This is expected, given that the solutions described in this paper and considered from theorem 1.1 are 1-periodic, in the sense that repeat identically in each stride. This difficulty of the model is evident in each of the cases described in figure 6.

At horizontal velocities equal to 2.06 ± 0.01 m s^{-1}, 3.07 ± 0.01 m s^{-1} and 4.07 ± 0.01 m s^{-1}, it was reported in [77] that the angular velocity $\dot{\alpha}$ of a human ($m = 77 \pm 9$ kg) running was 35.67 ± 9.5 deg s^{-1}, 57.37 ± 13.2 deg s^{-1} and 82.27 ± 19.7 deg s^{-1}, respectively, with $k_{\text{norm}} := kl_0/(\text{mg}) = 21.57 \pm 2.2$, 21.07 ± 3.4 and 21.37 ± 4.5, respectively. In all these cases the parameter conditions valid for theorem 1.1 are largely valid, as $k/m - \omega^2 \gg 0$, if we believe that an accurate estimate of ω is $\dot{\alpha}$. The same assessment is valid if we consider the parameters available in [77] for the pheasant. Although full data-supported information is not available in the literature (as far as we know), it seems reasonable to us to infer that the range of parameters for which we proved the existence of smooth solutions includes values of biomechanical parameters valid when many animals, such as bipedal birds, are running. Future studies would need to be dedicated to the proof of rigorous bounds to determine the range of parameters of validity of our approximation, but we also hope that corresponding experiments determining biological quantities of interest become more wide spread.

The functional form of the time duration of the stance phase τ^* is interesting, because the dependence on the normalized stiffness decouples from the other parameters. Note that in previous studies (e.g. [11,24]), the shape of the estimate of this quantity based on the model proposed was extremely complicated. This suggest a potential strategy to model the angle swept during stance as an inverse root of the normalized stiffness times a function which depends on the velocity at touchdown and the the Froude number. The validity of this idea needs to be tested on more data coming from different animal species, such as human and bipedal birds. It would be interesting to develop an extension of this model for other gaits, including bipedal walking or more complex quadrupedal motions.

With respect to the SLIP model, our model seems to indicate that human running adheres to additional dynamical constraints [24], ultimately further characterizing human running. Our analytic and simulation studies, together with the data analysed, show that vertical displacement of the CoM during running can be described by a model that is of lower dimension than SLIP. Moreover, a smooth running gait (no abrupt changes in velocity during switch between phases)

requires further parameter constraints (see theorem 1.1). Similarly to SLIP, our model implies that not all limb movements are dynamically feasible or self-stabilizing for a given body mass and leg length, so it would be interesting to verify in detail if similar leg kinematics and elastic properties, as described by our model, are valid across taxa (e.g. other mammals, bipedal birds). This idea comes from the mathematical deductions derived from our model assumptions combined with ideas from SLIP literature [10], more than from direct biological insight, and we do not extensively test this for our model in the present manuscript.

7. Conclusion

In this paper, we study a hybrid dynamical system that results from a reduction of the spring-loaded inverted pendulum model under the assumption of constant angular velocity during stance. We provide theoretical results, such as existence, non-existence and multiplicity of smooth solutions. We describe numerical simulations validating our theorem and we demonstrate the performance of our model on data from experiments on human running on treadmill and overground at comfortable and fast speed. Our results are interesting because of the simplicity of the model, the accuracy in fitting data from varied experiments, and because explicit formulas for biomechanical parameters (e.g. duration of the stance phase) can be explicitly computed. The model is valid without the restriction of small compression and tends to decrease its performance when fitted on real data if the motion across strides substantially departs from periodicity.

Data accessibility. The dataset used in this paper is taken from references [73,74] and is publicly available.

The data are provided in the electronic supplementary material [78].

Declaration of AI use. Yes, we have used AI-assisted technologies in creating this article. Simulations have used a response from ChatGPT on 20250116 with prompt: "Can you please provide a Python code that simulates solutions to the spring-loaded inverted pendulum model for running? Can you include in the simulation multiple aerial and stance phases?" The code did not provide the correct equations of motion and was modified to simulate the proposed dynamical system by A.M.S. The final code is available with the manuscript.

Authors' contributions. A.M.S.: conceptualization, data curation, formal analysis, funding acquisition, investigation, methodology, project administration, resources, software, supervision, validation, visualization, writing—original draft, writing—review and editing; K.L.F.: conceptualization, funding acquisition, project administration, supervision, visualization, writing—review and editing.

Both authors gave final approval for publication and agreed to be held accountable for the work performed therein.

Conflict of interest declaration. We declare we have no competing interests.

Funding. A.M.S. and K.L.F. are supported by the collaborative NSF Awards no. 2152789 and no. 2152792 on RUI: Collaborative Research: DMS/NIGMS 1: The mathematical laws of morphology and biomechanics through ontogeny.

Acknowledgements. We thank the referees and the editors for their work and valuable comments.

References

1. Gordon MS, Blickhan R, Dabiri JO, Videler JJ. 2017 *Animal locomotion: physical principles and adaptations*, 1st edn. Boca Raton: CRC Press.
2. Holmes P, Full RJ, Koditschek D, Guckenheimer J. 2006 The dynamics of legged locomotion: models, analyses, and challenges. *SIAM Rev.* **48**, 207–304. (doi:10.1137/S0036144504445133)
3. McGeer T. 1990 Passive dynamic walking. *Int. J. Rob. Res.* **9**, 62–82. (doi:10.1177/027836499000900206)
4. McGeer T. 1990 Passive bipedal running. *Proc. R. Soc. Lond. B* **240**, 107–134. (doi:10.1098/rspb.1990.0030)
5. Raibert MH. 1986 *Legged robots that balance*. Cambridge, UK: MIT Press.
6. Raibert M, Blankespoor K, Nelson G, Playter R. 2008 Bigdog, the Rough-Terrain quadruped robot. *IFAC Proc. Vol.* **41**, 10822–10825. (doi:10.3182/20080706-5-KR-1001.01833)

7. Westervelt ER, Grizzle JW, Koditschek DE. 2003 Hybrid zero dynamics of planar bipedal walkers. *IEEE Trans. Autom. Control* **48**, 42–56. (doi:10.1109/TAC.2002.806653)
8. Blickhan R. 1989 The spring-mass model for running and hopping. *J. Biomech.* **22**, 1217–1227. (doi:10.1016/0021-9290(89)90224-8)
9. Blickhan R, Full RJ. 1993 Similarity of multilegged locomotion: Bouncing like a monopode. *J. Comp. Physiol. A* **173**, 509–517. (doi:10.1007/BF00197760)
10. Full RJ, Koditschek DE. 1999 Templates and anchors: neuromechanical hypotheses of legged locomotion on land. *J. Exp. Biol.* **202**, 3325–3332. (doi:10.1242/jeb.202.23.3325)
11. Geyer H, Seyfarth A, Blickhan R. 2005 Spring-mass running: simple approximate solution and application to gait stability. *J. Theor. Biol.* **232**, 315–328. (doi:10.1016/j.jtbi.2004.08.015)
12. McMahon TA, Cheng GC. 1990 The mechanism of running: how does stiffness couple with speed?. *J. Biomech.* **23**, 65–78. (doi:10.1016/0021-9290(90)90042-2)
13. Delp S. 2023 Mobilize Center. See https://mobilize.stanford.edu/ (retrived 22nd June 2023).
14. Ernst M, Götze M, Müller R, Blickhan R. 2014 Vertical adaptation of the center of mass in human running on uneven ground. *Hum. Mov. Sci.* **38**, 293–304. (doi:10.1016/j.humov.2014.05.012)
15. Saunders JDM, Inman VT, Eberhart HD. 1953 The major determinants in normal and pathological gait. *J. Bone Joint Surg.* **35A**, 543–728. (doi:10.2106/00004623-195335030-00003)
16. Alexander RMN. 1984 The gaits of bipedal and quadrupedal animals. *Int. J. Rob. Res.* **3**, 49–59. (doi:10.1177/027836498400300205)
17. Alexander RM. 2003 *Principles of animal locomotion*. Princeton: Princeton University Press.
18. Farley CT, Blickhan R, Saito J, Taylor CR. 1991 Hopping frequency in humans: a test of how springs set stride frequency in bouncing gaits. *J. Appl. Physiol.* **71**, 2127–2132. (doi:10.1152/jappl.1991.71.6.2127)
19. Farley CT, Glasheen J, McMahon TA. 1993 Running springs: speed and animal size. *J. Exp. Biol.* **185**, 71–86. (doi:10.1242/jeb.185.1.71)
20. Ruina A. 1998 Non-holonomic stability aspects of piecewise holonomic systems. *Rep. Math. Phys.* **42**, 91–100. (doi:10.1016/S0034-4877(98)80006-2)
21. Selvitella AM, Foster KL. 2022 The spring-mass model and other reductionist models of Bipedal locomotion on inclines. *Integr. Comp. Biol.* **62**, 1320–1334. (doi:10.1093/icb/icac047)
22. Selvitella AM, Foster KL. 2022 Gait stability of the spring-mass model of planar locomotion on inclines. *Integr. Comp. Biol.* **62**, S99-S99. (doi:10.1093/icb/icac047)
23. Selvitella AM, Foster KL. 2023 On the variability and dependence of human leg stiffness across strides during running and some consequences for the analysis of locomotion data. *R. Soc. Open Sci.* **10**, 230597. (doi:10.1098/rsos.230597)
24. Selvitella AM, Foster KL. 2024 An approximate solution of the SLIP model under the regime of linear angular dynamics during stance and the stability of symmetric periodic running gaits. *J. Theor. Biol.* **595**, 111934. (doi:10.1016/j.jtbi.2024.111934)
25. Alexander RM. 1981 The gaits of tetrapods: adaptations for stability and economy. *Symposia Zool. Soc. Lond.* **48**, 269–287.
26. Alexander RM. 1989 Optimization and gaits in the locomotion of vertebrates. *Physiol. Rev.* **69**, 1199–1227. (doi:10.1152/physrev.1989.69.4.1199)
27. Patek SN, Biewener AA. 2018 *Animal locomotion*, 2nd edn. Oxford, UK: Oxford University Press.
28. Dickinson MH, Farley CT, Full RJ, Koehl MA, Kram R, Lehman S. 2000 How animals move: an integrative view. *Science* **288**, 100–106. (doi:10.1126/science.288.5463.100)
29. Foster KL, Collins CE, Higham TE, Garland Jr T. 2015 Determinants of lizard escape performance: decision, motivation, ability, and opportunity. In *Escaping from Predators: An Integrative View of Escape Decisions* (eds WE Cooper Jr, DT Blumstein), pp. 287–321. Cambridge, UK: Cambridge University Press.
30. Garland Jr T, Losos JB. 1994 Ecological morphology of locomotor performance in squamate reptiles. In *Ecological Morphology: Integrative Organismal Biology* (eds PC Wainwright, SM Reilly), pp. 240–302. Chicago, IL: University of Chicago Press.
31. Arnold SJ. 1983 Morphology, performance and fitness. *Am. Zool.* **23**, 347–361. (doi:10.1093/icb/23.2.347)
32. Garland T. 1983 The relation between maximal running speed and body mass in terrestrial mammals. *J. Zool.* **199**, 157–170. (doi:10.1111/j.1469-7998.1983.tb02087.x)
33. Losos JB. 1990 The evolution of form and function: morphology and locomotor performance in West Indian *Anolis Lizards*. *Evolution* **44**, 1189–1203. (doi:10.2307/2409282)

34. Lovejoy CO. 1988 Evolution of human walking. *Sci. Am.* **259**, 118–125. (doi:10.1038/scientificamerican1188-118)
35. Scales JA, Butler MA. 2016 Adaptive evolution in locomotor performance: how selective pressures and functional relationships produce diversity. *Evolution* **70**, 48–61. (doi:10.1111/evo.12825)
36. Vanhooydonck B, Van Damme R. 2001 Evolutionary trade–offs in locomotor capacities in lacertid lizards: are splendid sprinters clumsy climbers? *J. Evol. Biol.* **14**, 46–54. (doi:10.1046/j.1420-9101.2001.00260.x)
37. Birn-Jeffery AV, Hubicki CM, Blum Y, Renjewski D, Hurst JW, Daley MA. 2014 Don't break a leg: running birds from quail to ostrich prioritise leg safety and economy on uneven terrain. *J. Exp. Biol.* **217**, 3786–3796. (doi:10.1242/jeb.102640)
38. Foster KL, Selvitella AM. 2022 Transfer of anolis locomotor behavior across environments and species. *Integr. Comp. Biol.* **62**, 774–790. (doi:10.1093/icb/icac015)
39. Foster KL, Selvitella AM. 2022 Anolis ecomorph biomechanics across arboreal environments: What can machine learning tell us about behavioral plasticity in lizards?. *Integr. Comp. Biol.* **62**, S99-S99. (doi:10.1093/icb/icac015)
40. Müller R, Birn-Jeffery AV, Blum Y. 2016 Human and avian running on uneven ground: a model-based comparison. *J. R. Soc. Interface* **13**, 20160529. (doi:10.1098/rsif.2016.0529)
41. Alexander RM. 2003 Modelling approaches in biomechanics. *Phil. Trans. R. Soc. Lond. B* **358**, 1429–1435. (doi:10.1098/rstb.2003.1336)
42. Geyer H, Seyfarth A, Blickhan R. 2006 Positive force feedback in bouncing gaits? *Proc. R. Soc. B* **270**, 2173–2183. (doi:10.1098/rspb.2003.2454)
43. Ghigliazza P, Holmes RM. 2005 Towards a neuromechanical model for insect locomotion: hybrid dynamical systems. *Regular Chaotic Dyn.* **10**, 193–225. (doi:10.1070/RD2005v010n02ABEH000311)
44. Cavagna GA, Margaria R. 1966 Mechanics of walking. *J. Appl. Physiol.* **21**, 271–278. (doi:10.1152/jappl.1966.21.1.271)
45. Cavagna GA, Margaria R, Saibene FP. 1963 External work in walking. *J. Appl. Physiol.* **18**, 1–9. (doi:10.1152/jappl.1963.18.1.1)
46. Cavagna GA, Heglund NC, Taylor CR. 1977 Mechanical work in terrestrial locomotion: two basic mechanisms for minimizing energy expenditure. *Am. J. Physiol.* **233**, R243–R261. (doi:10.1152/ajpregu.1977.233.5.R243)
47. Margaria R. 1976 *Biomechanics and energetics of muscular exercise*. Oxford: Clarendon Press.
48. Geyer H, Seyfarth A, Blickhan R. 2006 Compliant leg behaviour explains basic dynamics of walking and running. *Proc. R. Soc. B* **273**, 2861–2867. (doi:10.1098/rspb.2006.3637)
49. Rummel J, Seyfarth A. 2008 Stable running with segmented legs. *Int. J. Rob. Res.* **27**, 919–934. (doi:10.1177/0278364908095136)
50. Seipel JE, Holmes P. 2005 Running in three dimensions: analysis of a point-mass sprung-leg model. *Int. J. Rob. Res.* **24**, 657–674. (doi:10.1177/0278364905056194)
51. Whittacker ET. 1904 *A treatise on the analytical dynamics of particles and rigid bodies*, 4th edn. New York, NY: Cambridge University Press.
52. Goebel R, Sanfelice RG, Teel AR. 2012 *Hybrid dynamic systems: modeling, stability, and robustness*. Princeton: Princeton University Press.
53. van der Schaft A, Schumacher H. 2000 *An introduction to hybrid dynamical systems*. London, UK: Springer.
54. Ghigliazza RM, Altendorfer R, Holmes P, Koditschek DE. 2003 A simply stabilized running model. *SIAM J. Appl. Dyn. Syst.* **2**, 187–218. (doi:10.1137/S1111111102408311)
55. Seyfarth A, Geyer H, Günther M, Blickhan R. 2002 A movement criterion for running. *J. Biomech.* **35**, 649–655. (doi:10.1016/S0021-9290(01)00245-7)
56. Mawhin J. 1988 The forced pendulum equation: a paradigm fo nonlinear analysis and dynamical systems. *Expositiones Math.* **6**, 271–287.
57. Ortega R, Serra E, Tarallo M. 2000 Non-continuation of the periodic oscillations of a forced pendulum in the presence of friction. *Proc. Am. Math. Soc.* **128**, 2659–2665. (doi:10.1090/S0002-9939-00-05389-2)
58. Torres P. 2023 A non-existence result for periodic solutions of the relativistic pendulum with friction. *Appl. Math. Lett.* **144**, 108697. (doi:10.1016/j.aml.2023.108697)
59. Schwind WJ, Koditschek DE. 2000 Approximating the stance map of a 2-DOF monoped runner. *J. Nonlinear Sci.* **10**, 533–568. (doi:10.1007/s004530010001)

60. Płociniczak L, Wróblewska Z. 2020 Solution and asymptotic analysis of a boundary value problem in the spring-mass model of running. *Nonlinear Dyn.* **99**, 2693–2705. (doi:10.1007/s11071-019-05462-z)
61. Wróblewska Z, Kowalczyk P, Płociniczak L. 2020 Stability of fixed points in an approximate solution of the spring-mass running model. *IMA J. Appl. Math.* **88**, 429–454. (doi:10.1093/imamat/hxad014)
62. Gullstrand L, Halvorsen K, Tinmark F, Eriksson M, Nilsson J. 2009 Measurements of vertical displacement in running, a methodological comparison. *Gait Posture* **30**, 71–75. (doi:10.1016/j.gaitpost.2009.03.001)
63. van Oeveren BT, de Ruiter CJ, Beek PJ, van Dieën JH. 2021 The biomechanics of running and running styles: a synthesis. *Sports Biomech.* **23**, 516–554. (doi:10.1080/14763141.2021.1873411)
64. da Rosa RG, Oliveira HB, Gomeñuka NA, Masiero MPB, da Silva ES, Zanardi APJ, de Carvalho AR, Schons P, Peyré-Tartaruga LA. 2019 Landing-takeoff asymmetries applied to running mechanics: a new perspective for performance. *Front. Physiol.* **10**, 415. (doi:10.3389/fphys.2019.00415)
65. Farley CT, Gonzalez O. 1996 Leg stiffness and stride frequency in human running. *J. Biomech.* **29**, 181–186. (doi:10.1016/0021-9290(95)00029-1)
66. Halvorsen K, Eriksson M, Gullstrand L. 2012 Acute effects of reducing vertical displacement and step frequency on running economy. *J. Strength Cond Res.* **26**, 2065–2070. (doi:10.1519/JSC.0b013e318239f87f)
67. He JP, Kram R, McMahon TA. 1991 Mechanics of running under simulated low gravity. *J. Appl. Physiol.* **71**, 863–870. (doi:10.1152/jappl.1991.71.3.863)
68. Lee CR, Farley CT. 1998 Determinants of the center of mass trajectory in human walking and running. *J. Exp. Biol.* **201**, 2935–2944. (doi:10.1242/jeb.201.21.2935)
69. Novacheck TF. 1998 The biomechanics of running. *Gait Posture* **7**, 77–95. (doi:10.1016/S0966-6362(97)00038-6)
70. Fukuchi RK, Fukuchi CA, Duarte M. 2017 A public dataset of running biomechanics and the effects of running speed on lower extremity kinematics and kinetics. *PeerJ* **5**, e3298. (doi:10.7717/peerj.3298)
71. Fukuchi RK, Fukuchi CA, Duarte M. 2017 A public dataset of running biomechanics and the effects of running speed on lower extremity kinematics and kinetics. (doi:10.6084/m9.figshare.4543435)
72. Alexander RMN. 1995 Leg design and jumping technique for humans, other vertebrates and insects. *Phil. Trans. R. Soc. Lond. B* **347**, 235–248. (doi:10.1098/rstb.1995.0024)
73. Riglet L, Delphin C, Claquesin O, Laroche D, Gueugnon M. 2024 3D motion analysis dataset of healthy young adult volunteers walking and running on overground and treadmill. *Sci. Data* **11**, 556. (doi:10.1038/s41597-024-03420-y)
74. Riglet L, Delphin C, Claquesin L, Orliac B, Ornetti P, Laroche D, Gueugnon M. 2024 3D motion analysis dataset of healthy young adult volunteers walking and running on overground and treadmill. Figshare. Collection. (doi:10.6084/m9.figshare.c.7056797)
75. Cox D, Little J, O'Shea D. 2005 *Using algebraic geometry*. Berlin, Germany: Springer Science+Business Media.
76. Fulton W, Weiss R. 1974 *Algebraic curves: an introduction to algebraic geometry*. San Francisco (USA): W. A. Benjamin Publisher.
77. Blum Y, Birn-Jeffery AV, Daley MA, Seyfarth A. 2011 Does a crouched leg posture enhance running stability and robustness? *J. Theor. Biol.* **281**, 97–106. (doi:10.1016/j.jtbi.2011.04.029)
78. Selvitella AM, Foster KL. 2025 Sharp conditions for the existence and multiplicity of smooth periodic solutions to a hybrid dynamical system for human running. Figshare. (doi:10.6084/m9.figshare.c.8061265)